Chemical Engineering Journal 349 (2018) 168–175

Contents lists available at ScienceDirect

Chemical Engineering Journal

journal homepage: www.elsevier.com/locate/cej

# A novel stretchable supercapacitor electrode with high linear capacitance

Xiang Chu[a], Haitao Zhang[a,*], Hai Su[a], Fangyan Liu[a], Bingni Gu[a], Haichao Huang[a], Hepeng Zhang[a], Wen Deng[a], Xiaotong Zheng[a], Weiqing Yang[a,b,*]

[a] Key Laboratory of Advanced Technologies of Materials (Ministry of Education), School of Materials Science and Engineering, Southwest Jiaotong University, Chengdu 610031, PR China

[b] State Key Laboratory of Traction Power, Southwest Jiaotong University, Chengdu 610031, China

## HIGHLIGHTS

- Growth of hierarchical carbon tubular nanostructures onto spring substrate.
- In-situ synthesis of polyaniline nanoparticles onto carbonaceous materials.
- Highly stretchable supercapacitor electrode based on stainless steel spring.
- Stable electrochemical performance of electrode under various deformations.

## GRAPHICAL ABSTRACT

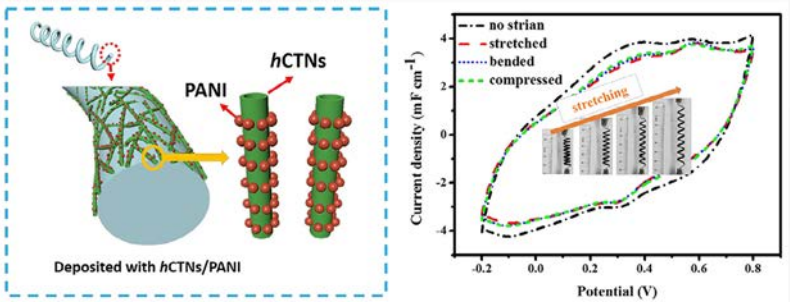


## ARTICLE INFO

*Keywords:*
Supercapacitor
Stretchability
Hierarchical structures
Carbon tubular nanostructures
Polyaniline

## ABSTRACT

Conventional flexible supercapacitors that can work under consecutive bending, folding and even twisting without performance degradation have been widely reported. Nevertheless, these devices can hardly be used under large tensile strain due to limited stretchability. In this regard, the application field of flexible supercapacitors can be remarkably broaden if they are designed as stretchable power supplies for wearable electronic devices. Herein, we report a stretchable supercapacitor electrode through in situ synthesis of hierarchical carbon tubular nanostructures (*h*CTNs) and conducting polyaniline (PANI) onto stainless steel spring (SSS) which features both excellent conductivity and high stretchability. The as-prepared helical electrode exhibits considerable specific capacitance of 277.8 F $g^{-1}$ at 1 A $g^{-1}$ and unprecedented linear capacitance of 402.8 mF $cm^{-1}$ at the current density of 1 mA $cm^{-1}$, which is much higher than most previously reported literatures. Besides, electrochemical performance of this electrode can be maintained under various mechanical loading such as compressing and bending. Additionally, 100% tensile strain of electrode is successfully demonstrated without sacrificing its electrochemical performance.

## 1. Introduction

Supercapacitors have garnered intense interest as an emerging class of energy storage device in the past decades attributed to high power density, moderate energy density, long cycling life and fast charge-discharge rate [1–3]. With the explosive development of portable and wearable electronics such as Apple Watch and Philips Fluid smartphone, the demand for portable power sources of light-weight and considerable flexibility has been further stimulated [4–8]. Till now, solid progress has been made towards flexible supercapacitors that can

* Corresponding authors at: Key Laboratory of Advanced Technologies of Materials (Ministry of Education), School of Materials Science and Engineering, Southwest Jiaotong University, Chengdu 610031, PR China (W. Yang).
*E-mail addresses:* haitaozhang@swjtu.edu.cn (H. Zhang), wqyang@swjtu.edu.cn (W. Yang).

https://doi.org/10.1016/j.cej.2018.05.090
Received 4 March 2018; Received in revised form 2 May 2018; Accepted 14 May 2018
Available online 15 May 2018
1385-8947/ © 2018 Published by Elsevier B.V.

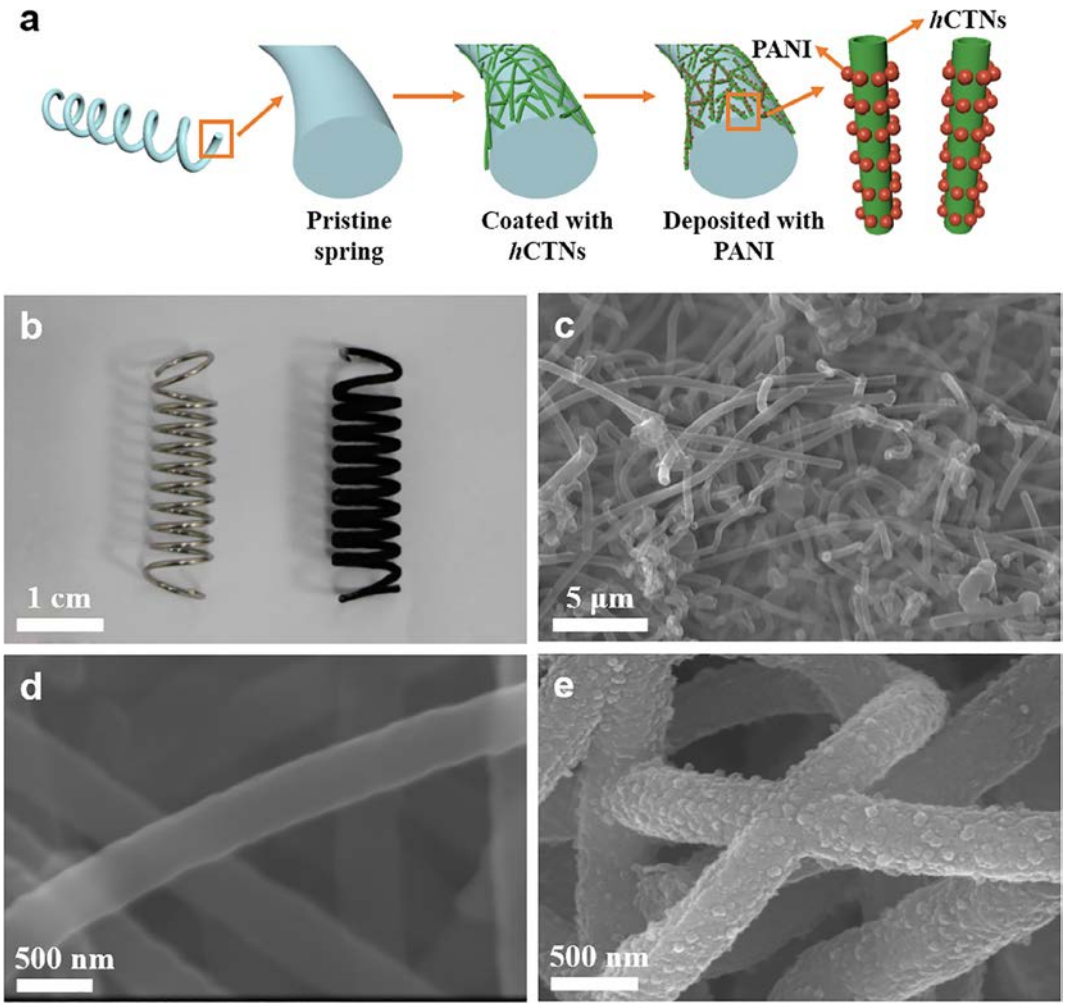


**Fig. 1.** (a) A schematic presentation of synthesizing *h*CTNs/PANI composites onto the surface of SSS substrates. (b) Digital image of pristine spring (left) and *h*CTNs coated spring (right). (c, d) SEM images of *h*CTNs at different magnifications. (e) SEM image of *h*CTNs/PANI composites.

work under consecutive bending, folding and even twisting without performance degradation [7,9–12]. However, supercapacitors with high stretchability have rarely been reported so far. Some advanced works have recently been reported to prepare stretchable supercapacitors, in which elastic fiber [13,14] or polymer film [15] were introduced as the substrates to provide stretchability. Nevertheless, stretchable substrates based on polymer are generally insulating and therefore an extra current collector needs to be integrated. Additionally, the stretchability of polymer-based substrate can often be perished due to the transition from elastic state to glass state at relatively low temperature, which severely restricts practical application of devices.

To assemble stretchable electrodes, some rational methods have been used through laminating thin film of electrochemical active materials onto stretchable substrates [16,17]. However, large interface resistance can be induced due to the existence of multiple interfaces between the electrode and the substrate. Obvious performance degradation can also be observed attributed to the delamination of active materials from the substrate. Other typical ways such as dip-coating [18] and electrochemical polymerization [19] methods have also been employed to deposit electrochemical active materials onto substrates. Nevertheless, compactness of obtained active materials loaded on substrates through these methods is not desirable. An ideal approach of fabricating stretchable electrode should minimize interface resistance and demonstrate desirable compactness of electrode synchronously. To this end, in-situ synthesis of electrode materials onto stretchable substrate can be a promising method. However, it still remains a great challenge to in-situ synthesize active materials onto the surface of various stretchable substrates to date, especially for substrates with irregular shape and large radius of curvature.

Herein we have developed a novel stretchable supercapacitor electrode through in-situ synthesis of hierarchical carbon tubular nanostructures (*h*CTNs) and conducting polyaniline (PANI) composites onto stainless steel spring (SSS) substrate. The as-prepared electrode exhibits a considerable gravimetric capacitance of 277.8 F $g^{-1}$ at 1 A $g^{-1}$ and an unprecedented linear capacitance of 402.8 mF $cm^{-1}$ at the current density of 1 mA $cm^{-1}$ (in $H_2SO_4$ aqueous electrolyte), which is more than twice larger than that of pure *h*CTNs electrode and ~10 to 50 times higher than previously reported literatures [20–23]. Besides, the *h*CTNs/PANI electrode showed good cycling stability with 75% capacitance retention over 3000 charge/discharge cycles at a current density of 1 mA $cm^{-1}$. Furthermore, electrochemical performance of the helical electrode can be maintained under different mechanical loading such as compressing, bending and stretching. The electrode can also be easily stretched by 100% without obvious degradation in the structural integrity and electrochemical performance.

## 2. Experimental

### 2.1. Preparation of hCTNs onto SSS substrates

Commercial stretchable stainless springs with the size of

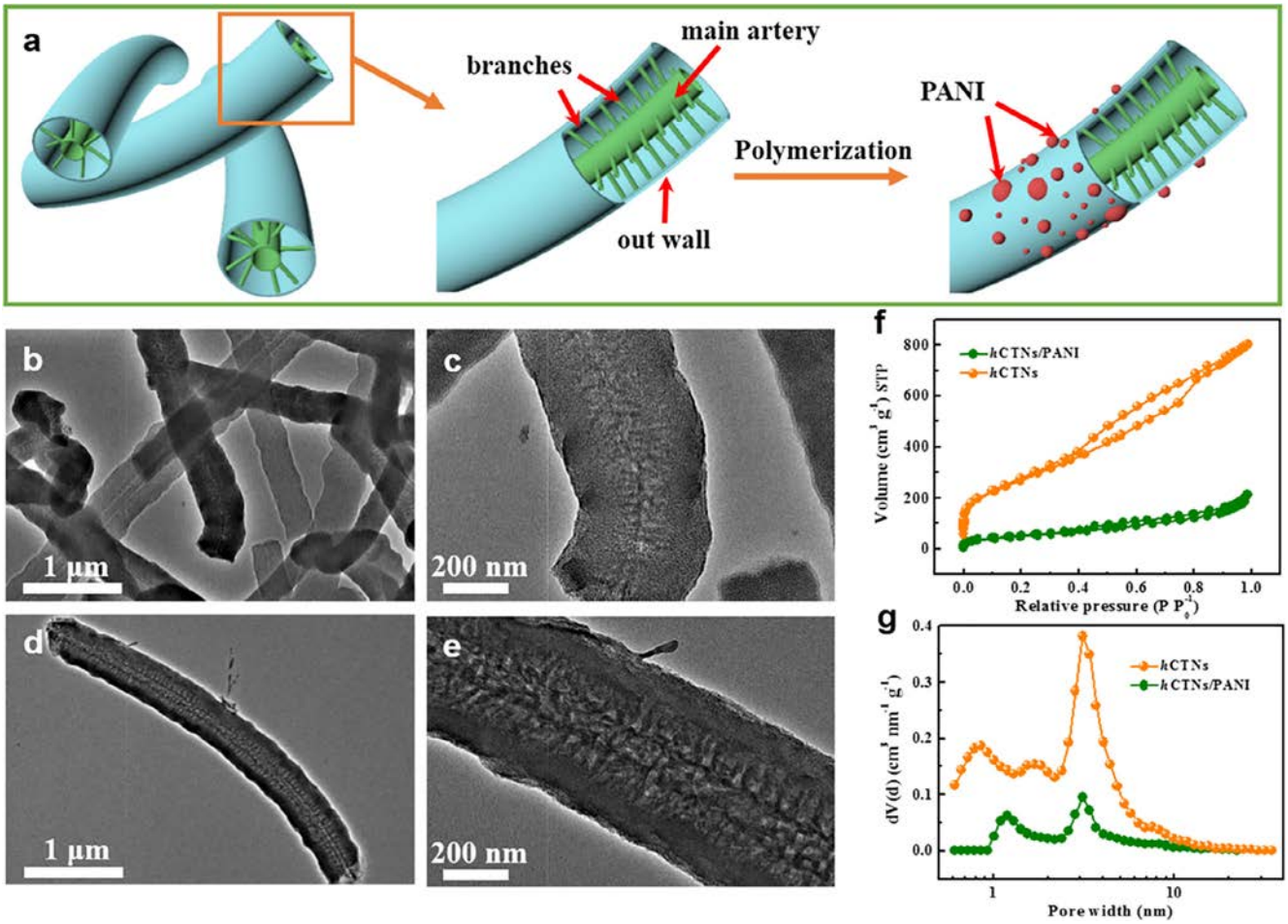


**Fig. 2.** (a) Schematic diagram of hierarchical structure of *h*CTNs tube and *h*CTNs/PANI composites. (b, c) TEM images of *h*CTNs tubes at different magnifications. (d, e) TEM images of *h*CTNs/PANI composites at different magnifications. (f) $N_2$ adsorption/desorption isotherms and (g) pore size distribution of *h*CTNs and *h*CTNs/PANI composites.

30 × 8 × 0.8 mm were rinsed with deionized water and alcohol in an ultrasonic cleaner for several times to remove contaminants on the surface and dried in oven, *h*CTNs were then synthesized onto the substrate through a simple reaction of Mg and $CO_2$. In a typical process, 4.0 g Mg powders with a purity of 99.5% were uniformly spread in the bottom of a high purity corundum boat with a size of 100 × 25 × 20 mm, SSS have to be tailored to better fit the size of the corundum boat prior to putting it on the top of the boat. Then the corundum boat with Mg powders in the bottom and spring on the top was put into a tube furnace (GSL-1700X, Hefei Kejing Materials Tech. Co., Ltd. China) with a multichannel flow controller (GMF-2Z, AnHui BEQ Equipment Tech. Co., Ltd. China) connected. The Mg powders were heated to an aimed temperature (800 °C) under the protection of Ar gas with a flow rate of 40 sccm. Once the aimed reaction temperature was achieved, the flow rate of Ar gas was switched to 20 sccm and $CO_2$ gas was blended as carbon source with an equivalent flow rate of Ar gas. After reacting for 1 h, spring based samples with uniform *h*CTNs coating can be obtained. To remove impurities including Mg and MgO, the as-prepared sample was dipped into 1 M HCl aqueous solution for 8 h, followed by washing with large quantity of deionized water and alcohol, and then naturally dried.

### 2.2. Preparation of hCTNs/PANI/spring and PANI/spring

PANI was in-situ polymerized according to ref. [5]. In a typical process, 36.5 μL of aniline (0.4 mmol) was added into 20 mL of 1 M $HClO_4$ aqueous solution to form solution A. 91.2 mg (0.27 mmol) of ammonium persulfate (APS) with a molar ratio between that of aniline and APS at 1:1 was dissolved in another 20 mL of 1 M $HClO_4$ aqueous solution to form solution B simultaneously. Subsequently, pristine spring or *h*CTNs/spring was placed into the above mentioned solution A. After which, solution B was added into solution A under magnetic stirring at room temperature and needed to keep 12 h to allow for complete PANI polymerization. After the reaction, the sample was taken out from the solution and washed by deionized water and alcohol for several times and dried naturally.

### 2.3. Data processing

To evaluate the electrochemical performance of every kind of electrode, capacitance was calculated from both galvanostatic discharge curves and cyclic voltammetry (CV) curves according to the following equation:

Linear capacitance calculated from discharge curves: $C = It/l\Delta V$

where $I$ (A) is the current used for the charge/discharge, $t$ (s) is the discharge time, $l$ (cm) is the length of spring coated with electrochemical materials and $\Delta V$ (V) is the voltage interval of the discharge.

Linear capacitance calculated from CV curves: $C = \frac{1}{v \cdot l \cdot \Delta V} \int_{V_0}^{V_0+\Delta V} i \, dV$

where $v$ (V/s) is the scan rate, $l$ (cm) is the length of spring coated with electrochemical materials, $V_0$ and $\Delta V$ (V) are initial potential and potential window of CV curves, $i$ (A) is the voltammetric discharge

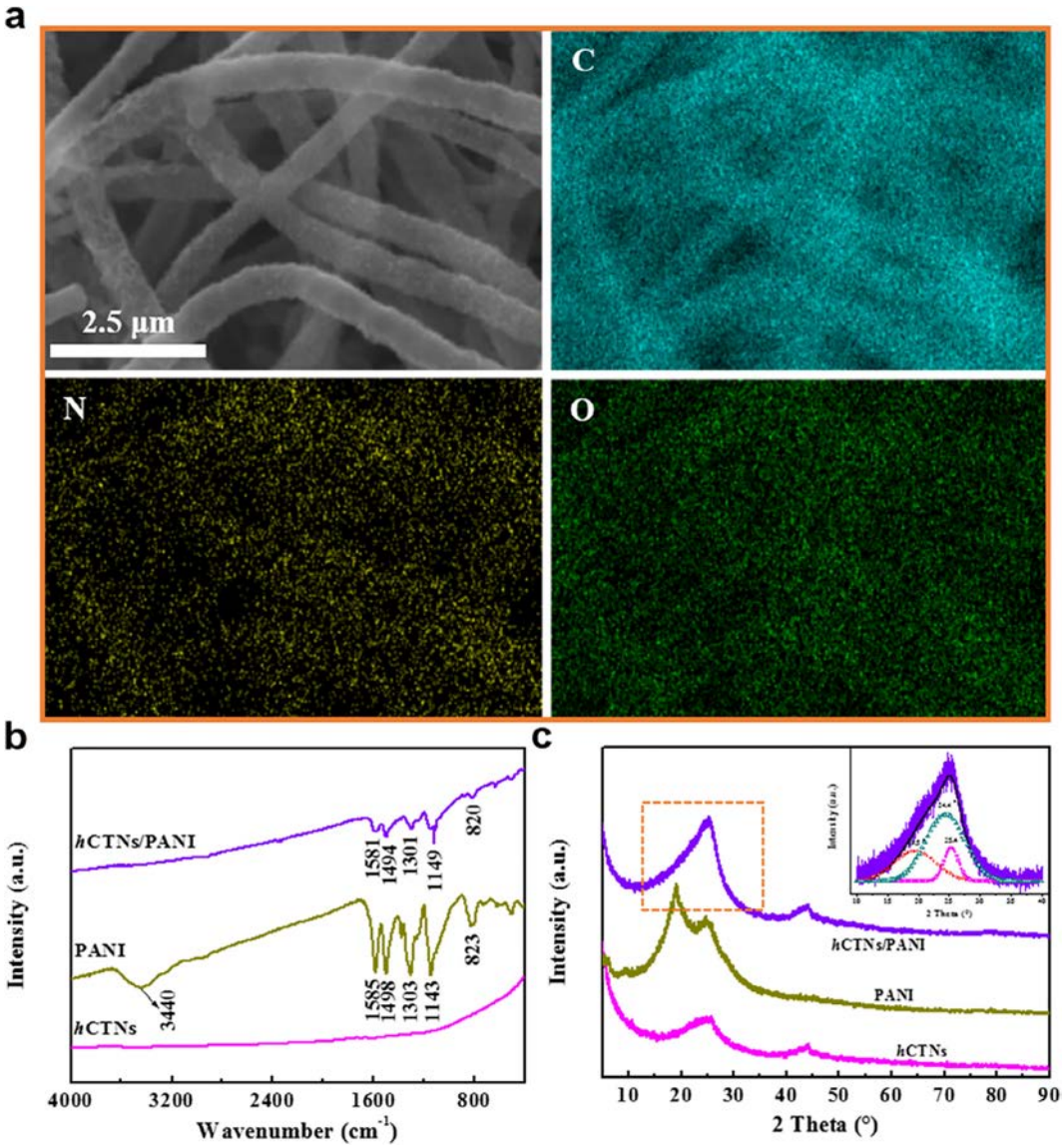


**Fig. 3.** (a) EDS mapping of *h*CTNs/PANI composites. (b) FTIR spectra and (c) XRD patterns of pure *h*CTNs, PANI and *h*CTNs/PANI composites. Inset: peak fitting of broad intense XRD peak appeared in the pattern of *h*CTNs/PANI composites at 25.3°, which can be regarded as an overlapped one consists of three narrow peaks located at 19.5°, 24.4° and 25.4°.

current.

Since the SSS substrate is not quite stable at high temperature especially under Mg atmosphere that possess strong reducibility, so the loading mass of electrochemical active materials can't simply be determined by subtracting the initial mass of substrate. That's why we mainly evaluate the performance of the electrode by linear capacitance rather than gravimetric capacitance. To point it out, gravimetric capacitance can be obtained through testing electrochemical performance of *h*CTNs and *h*CTNs/PANI powders, which was explicitly discussed in Supporting information.

### 2.4. Characterization of materials

Scanning electron microscopy (SEM) images were recorded using a FEI QUANTA FEG 250 SEM in the high-vacuum mode with an accelerating voltage of 20 kV. Transmission electron microscopy (TEM) and high-resolution TEM (HRTEM) characterizations were taken with a JEOL JEM-2100F instrument. Fourier transformed infrared (FTIR) spectra with a resolution of 2 $cm^{-1}$ were recorded on a Nicolet 6700 spectrometer (Thermo Fisher Scientific, US). X-ray diffraction (XRD) of the samples was carried out with PNAalytical X'Pert Powder diffractometer with Cu Kα radiation between 5° and 90°.

### 2.5. Electrochemical testing

The electrochemical tests are carried out in a three-electrode configuration, in which platinum foils and saturated calomel electrode (SCE) were used as counter and reference electrodes in 1 M $H_2SO_4$ aqueous electrolyte. Since the stainless steel spring can be used as current collector, the helical electrode can be directly tested in the three-electrode configuration by scraping *h*CTNs and *h*CTNs/PANI off from a length of spring and the bare length can be directly connected to three-electrode configuration. Cyclic voltammetry (CV) curves measured at the different scan rates ranging from 5 mV $s^{-1}$ to 50 mV $s^{-1}$, galvanostatic charge-discharge (GCD) process, electrochemical impedance spectroscopy (EIS) recorded in the frequency ranging from 100 kHz to 10 mHz with a 5 mV ac amplitude was carried out by a electrochemical workstation (CHI660E). The cycling life test was conducted on a LAND CT2001A battery testing system (Jin-nuo Wuhan Co., Ltd. China) by galvanostatic charge-discharge techniques at a current

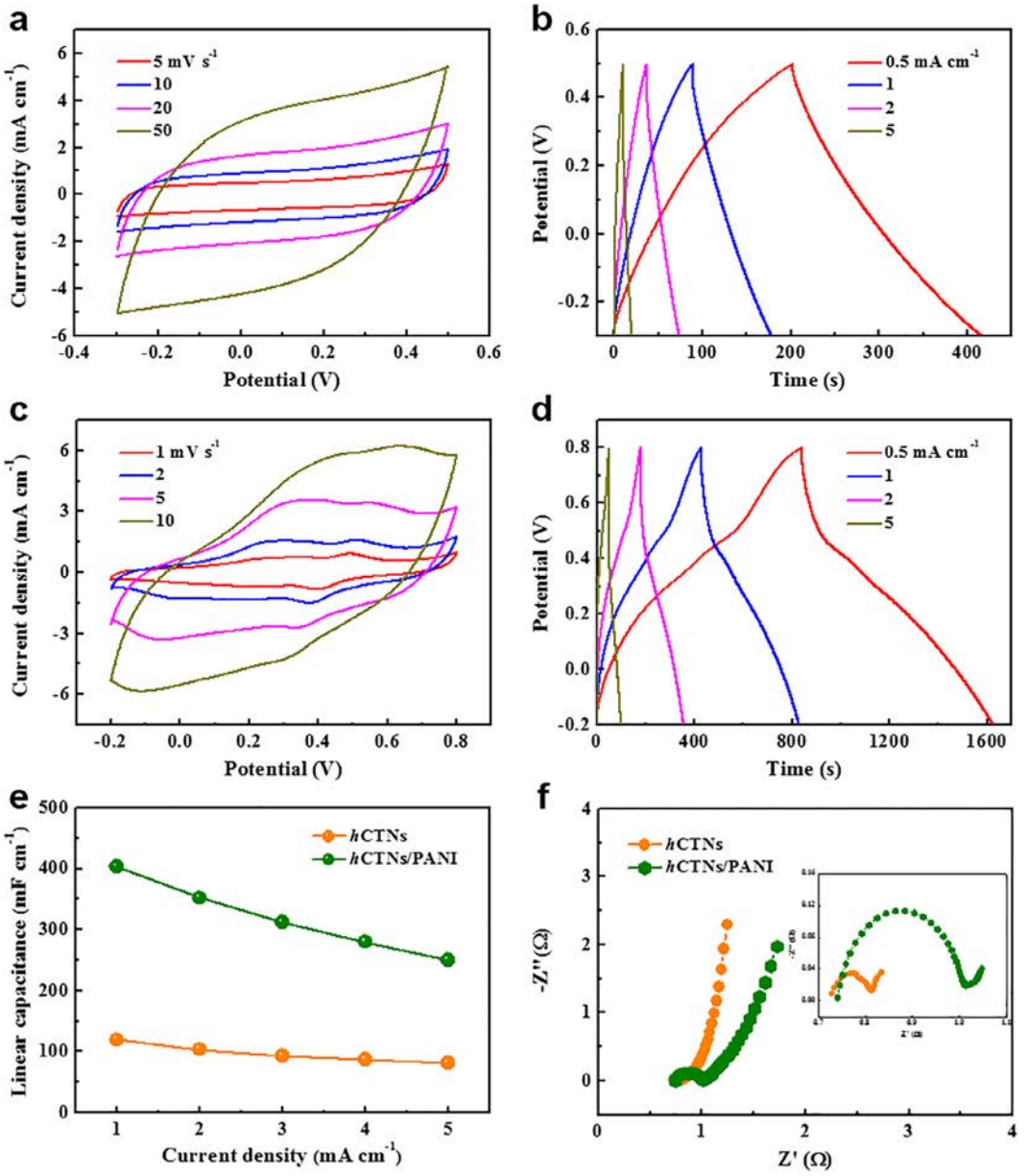


**Fig. 4.** (a) CV (5–50 mV $s^{-1}$ under −0.3–0.5 V) and (b) GCD (0.5–5 mA $cm^{-1}$) curves of *h*CTNs electrode. (c) CV (1–10 mV $s^{-1}$ under −0.2–0.8 V) and (d) GCD (0.5–5 mA $cm^{-1}$) curves of *h*CTNs/PANI electrode. (e) Linear capacitance plots of *h*CTNs and *h*CTNs/PANI electrode at different current densities derived from GCD curves. (f) Nyquist plots of electrodes based on *h*CTNs and *h*CTNs/PANI.

density of 1 mA $cm^{-1}$ with a potential window of −0.2 to 0.8 V.

## 3. Results and discussion

Inspired by the unique structure of ivy plants, in which stem networks closely attached onto ground could synergize with leaves covered above to make the best use of finite sunlight. Here we hypothesize electrochemical active composite materials with ivy-like structure could fully utilize the surface area of substrate and achieve sufficient contact with electrolyte. To prepare a stretchable electrode, a stainless steel spring (SSS) was introduced as stretchable substrate. The SSS features the capability for both considerable stretchability and high conductivity. Additionally, the stretchability of SSS substrate can be remained at a relatively wide temperature range.

For a typical fabrication of *h*CTNs/PANI hybrid electrode (Fig. 1a), stems-like hierarchical carbon tubular nanostructures (*h*CTNs) were firstly synthesized onto the surface of SSS through directly conversion of carbon dioxide using Mg powders as reductive agent (Fig. S1), which was reported in our previous work [24,25]. The formation mechanism of *h*CTNs can be generally proposed to a root-growth process, in which carbonaceous nucleuses are firstly formed on the rough surface of metallic magnesium liquid nanodroplets, the resultant *h*CTNs gradually come into formation along the axis of the nanotube from the root to the top with consecutive absorption of $CO_2$ molecules onto nucleuses (Fig. S2). The formation mechanism was expressly explained in both Supporting information and our previous work [25]. Nano-spherical polyaniline (PANI) playing the role of leaves was sequentially polymerized on *h*CTNs networks to form ivy-like structure via in-situ solution polymerization method. Fig. 1b shows digital image of *h*CTNs coated spring (right) and pristine spring (left), it can be clearly observed that *h*CTNs coated spring is darker and thicker in line than pristine spring, which means *h*CTNs have been uniformly attached on SSS substrate. SEM image of *h*CTNs at various magnifications are shown in Fig. 1c and Fig. S3, obviously *h*CTNs with the length of dozens of

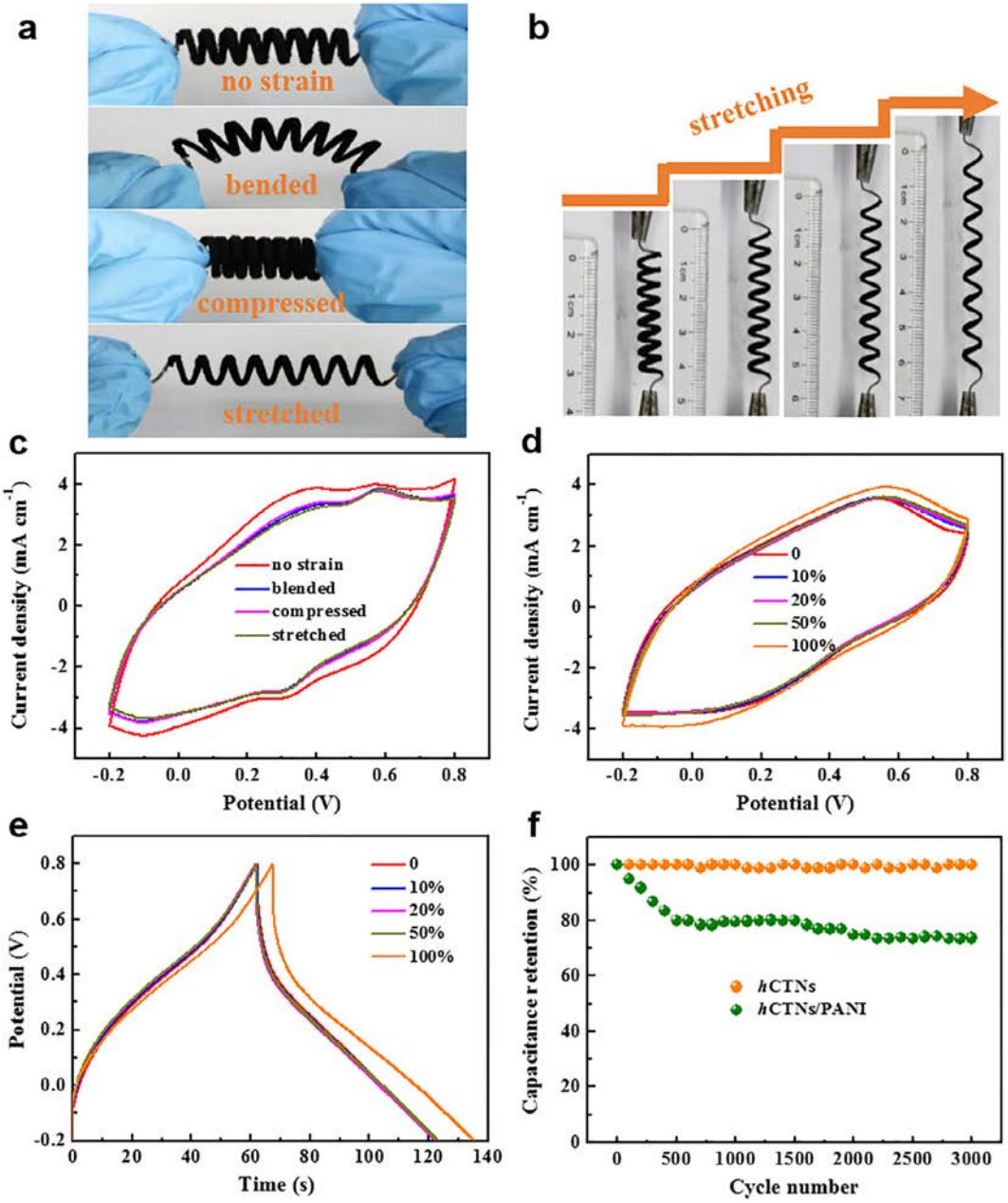


**Fig. 5.** (a) As-prepared *h*CTNs/PANI electrode can be mechanically compressed, bended and even stretched to a large strain (b) without obvious damage in structural integrity. (c) CV curves of *h*CTNs/PANI electrode under different mechanical loading. (d) CV and (e) GCD curves of *h*CTNs/PANI electrode with various strains from 10 to 100%. (f) Capacitance retention of *h*CTNs and *h*CTNs/PANI electrode (1 mA $cm^{-1}$).

micrometers are densely and randomly grown on the substrate. A single tube of *h*CTNs with relatively smooth surface and approximate 380 nm diameter is shown in Fig. 1d, which indicates larger size than single and multi-walled carbon nanotubes. The morphology of *h*CTNs/PANI composites was also characterized by SEM, the diameter of *h*CTNs tubes remain almost unchanged after coated with PANI, while the surface of the tubes become much rougher than that of pure *h*CTNs (Fig. 1e). Interestingly, a distinct intercross structure of *h*CTNs/PANI composites can be observed, of which the presence is of great benefit to charge transportation and stress transfer. The detailed nanostructure of *h*CTNs/PANI composites at larger magnification is shown in Fig. S4, obviously PANI nanoparticles with an approximate diameter of 80 nm were uniformly and stably wrapped on the surface of *h*CTNs, this structure is to a certain extent similar to that of ivy plants.

To further probe the inner structure of *h*CTNs and *h*CTNs/PANI composites, TEM characterization method was employed. Fig. 2 shows TEM images of *h*CTNs and *h*CTNs/PANI composites. Fig. 2a basically reveals the transformation in hierarchical structure of *h*CTNs and *h*CTNs/PANI. Generally, *h*CTNs possess a hierarchical multiple-tubes structure, which to a large extent looks like blood vessel spreading all over human body. There is a “main artery” run through the whole *h*CTNs and many “capillary vessels” branch out besides it. Fig. 2b, c show TEM images of *h*CTNs at different magnifications, in which *h*CTNs with uniform size and hierarchical structure can be observed. This hierarchical multiple-tubes structure can be demonstrated by more high quality TEM images of *h*CTNs in Fig. S5. Fig. 2d, e show TEM images of a single *h*CTNs/PANI tube at different magnifications, which inherits the intrinsic hierarchical structure of *h*CTNs. Fig. S6 shows more TEM images of *h*CTNs/PANI composites, we can conclude that the distinct hierarchical multiple-tubes structure of *h*CTNs can be well maintained after coated with PANI. Some differences can be traced between TEM images of *h*CTNs and *h*CTNs/PANI, we ascribe this change to the

absorption and polymerization of aniline monomer in the surface or within vessels of *h*CTNs. HRTEM image of *h*CTNs is shown in Fig. S7, in which many mesopores can be basically probed. According to BET data, the specific surface area (SSA) of *h*CTNs and *h*CTNs/PANI reach up to 984.5 $m^2 g^{-1}$ and 184.2 $m^2 g^{-1}$, respectively (Fig. 2f). The peak positions of *h*CTNs calculated by density functional theory model locate at about 0.9 and 3.1 nm, the peak positions of *h*CTNs/PANI locate at about 1.2 and 3.1 nm (Fig. 2g), which unambiguously demonstrates the existence of micro and mesopores in both *h*CTNs and *h*CTNs/PANI composites. As a result, hierarchical tubes in *h*CTNs naturally form channels for charge and ion transportation and the pores among "vessels" can benefit the penetration of electrolyte (Fig. S8), thus efficient electrochemical process and performance can be anticipated.

To investigate whether PANI has been successfully polymerized onto *h*CTNs, EDS mapping and FTIR spectra have been conducted. In the EDS mapping image of *h*CTNs/PANI composites (Fig. 3a), a uniform distribution of carbon and nitrogen element can be clearly observed, which is consistent with the morphology of the composites. The appearance of oxygen element can be attributed to either trace amount of $H_2O$ or oxygen-containing groups on the surface of *h*CTNs. FTIR spectra of pure *h*CTNs, pure PANI and *h*CTNs/PANI composites are depicted in Fig. 3b, the pure *h*CTNs exhibit no vibration modes in the range of 400–4000 $cm^{-1}$ because *h*CTNs are generally elementary substance of carbon and no chemical bond is existed in the matrix. In the spectra of pure PANI, the C═N and C═C stretchings of the quinonoid and benzenoid units appear at 1585 and 1498 $cm^{-1}$, respectively [26]. The band at 1303 $cm^{-1}$ is assigned to the C—N stretching of the benzenoid unit while the band at 1143 $cm^{-1}$ is due to the quinonoid unit of doped. The broad peak near 3440 $cm^{-1}$ is attributed to either —OH groups in $H_2O$ or N—H stretching of PANI and the peak at 823 $cm^{-1}$ is associated with the vibration of C—H stretching [27]. FTIR spectra of *h*CTNs/PANI composites exhibit characteristic bands of PANI, which confirms the presence of PANI component in the composites. XRD patterns of *h*CTNs, PANI and *h*CTNs/PANI composites are shown in Fig. 3c. Typical peaks of *h*CTNs appear at 2θ degree of about 25.4° and 44.2°, corresponding with (0 0 2) and (1 0 1) crystallographic planes. For pure PANI, the crystalline peaks centered at 19.7° and 24.6° are assigned to (0 2 0) and (2 0 0) reflections of PANI in emeraldine salt form [28]. In the pattern of *h*CTNs/PANI composites, a broad intense peak at 25.3° and weak peak at 44.1° can be clearly observed, which suggest that no additional crystalline order is introduced into the resulting nanocomposites [29,30]. Since the broad peak of *h*CTNs/PANI composites located at 25.3° is not strictly symmetric, we think it could be an overlapped one that contains several different peaks. Peak fitting result of this peak is exhibited in the inset of Fig. 3c, it can be clearly observed that the peak of *h*CTNs/PANI composites located at 25.3° can be perfectly divided into three narrow peaks: the peaks of 19.5° and 24.4° are corresponding to PANI component and the peak of 25.4° is ascribed to *h*CTNs component.

The electrochemical tests are carried out in a three-electrode configuration. Fig. 4a, b show the cyclic voltammetry (CV) and galvanostatic charge-discharge (GCD) curves of pure *h*CTNs electrode, respectively. Obviously, CV curves of *h*CTNs share a rectangular shape and GCD curves exhibit the typical triangle-shape charge-discharge profiles that corresponds to an electrical double-layer capacitor [31,32]. After coated with PANI, the potential window of *h*CTNs electrode can be broadened. Fig. 4c depicts the CV curves of *h*CTNs/PANI hybrid electrode at various scan rate with broader potential window, the characteristic redox peaks of PANI can be clearly observed, originating from the transformation among the leucoemeraldine base (LB), the emeraldine salt (ES), and the pernigraniline base (PB) [5,21,33]. The current density increases along with increasing scan rate, suggesting good rate capability [34]. To reveal the detailed capacitive behavior, GCD curves of *h*CTNs/PANI hybrid electrode at various current densities are presented in Fig. 4d, in which *h*CTNs/PANI composites demonstrate much longer discharging time than the *h*CTNs at the same current density. It means that the former one exhibits higher specific capacitance values than the latter. The linear capacitance plots derived from the charge/discharge curves are shown in Fig. 4e. The linear capacitance of bare *h*CTNs derived from galvanostatic discharge curve was calculated to be 119.6 mF $cm^{-1}$, while the value increased to an unprecedented high level of 402.8 mF $cm^{-1}$ after coated with PANI nanoparticles (the measured current density is 1 mA $cm^{-1}$), which is more than twice times larger than former one. Integrating of CV curves also suggests that the linear capacitance of *h*CTNs electrode (120.3 mF $cm^{-1}$ at a scan rate of 5 mV $s^{-1}$) can be remarkably enhanced through coated with PANI (461.8 mF $cm^{-1}$ at 5 mV $s^{-1}$). This value is about 10 to 50 times higher than all previously reported literatures (Table S1). Besides, the *h*CTNs/PANI composites also show a considerable gravimetric capacitance of 277.8 F $g^{-1}$ at 1 A $g^{-1}$, which is also much higher than that of pure *h*CTNs (63.8 F $g^{-1}$ at 1 A $g^{-1}$). To point it out, we have researched the influence of polymerization time on electrochemical performance of *h*CTNs/PANI hybrid electrode. As shown in Fig. S9, with the increasing of polymerization time from 0.5 h to 12 h, the linear capacitance of *h*CTNs/PANI hybrid electrode increases from 95.6 mF $cm^{-1}$ to 402.8 mF $cm^{-1}$, which can be attributed to increased loading mass of PANI on *h*CTNs. Since the polymerization time reaches up to 6 h or longer one, the linear capacitance comes to saturated state due to complete polymerization of aniline monomer. Herein, we attribute the remarkable enhancement in capacitance of *h*CTNs/PANI hybrid electrode to the pseudocapacitance of PANI and synergistic effect of PANI and *h*CTNs. On one hand, pseudocapacitive PANI figures large capacitance due to multiple intrinsic redox states. On the other hand, *h*CTNs network plays the role of conductive scaffold and upholder for PANI, which can substantially facilitate collection of the redox current of PANI and increase the loading mass of electrochemical active material (the average loading mass of *h*CTNs/PANI composite was evaluated to be 1.31 mg $cm^{-1}$). Moreover, the PANI in granular shape with small diameter (~80 nm) further increase the exposed electrochemical surface area of active material in electrolyte, hence effective use of active material can be anticipated. Electrochemical kinetics and ionic resistance were studied by electrochemical impedance spectroscopy (EIS). The semicircle in the EIS plots of pure PANI electrode (Fig. S10) reveals a relative large charge-transfer resistance (26.3 Ω), indicating an unfavorable charge-transfer kinetics for pure PANI electrode. EIS plots of *h*CTNs and *h*CTNs/PANI electrodes were recorded in Fig. 4f, the nearly vertical shape of obtained curves at lower frequencies indicates an ideal capacitive behavior of both *h*CTNs and *h*CTNs/PANI electrode [24,35]. Equivalent series resistance (ESR) of *h*CTNs and *h*CTNs/PANI composite extracted from high frequency ($10^5$ Hz) are estimated to be ~0.73 and ~0.74 Ω, respectively. Moreover, the *h*CTNs/PANI electrode demonstrated a much lower charge-transfer resistance (0.27 Ω) than pure PANI electrode, which further confirmed that the conductivity of conducting polymer could be largely increased through hybridizing with carbonaceous materials.

To further demonstrate the potential of *h*CTNs/PANI hybrid electrode for practical application, mechanical properties and cycling performance of as-prepared electrode were investigated. According to Fig. 5a, this as-prepared helical electrode can be mechanically compressed, bended and stretched without sacrificing its structural integrity. Particularly, this electrode can endure a wide range of tensile strain from 10 to 100%, which endow them great potential for practical application (Fig. 5b). Fig. 5c further depicts CV curves of *h*CTNs/PANI hybrid electrode under various loadings, from which we can conclude that electrochemical performance of *h*CTNs/PANI electrode can be remained almost unchanged under various mechanical loading such as compressing, bending and stretching. CV and GCD curves of *h*CTNs/PANI electrode with various strains are traced in Fig. 5d and e, respectively. The shape of CV and GCD curves can be well maintained over a wide range of tensile strains from 10% to 100%, which means the electrode can keep electrochemical stability even at large strain. Cycling performance was tested by 3000 charge-discharge cycles at the

current density of 1 mA cm$^{-1}$. The capacitance retention of *h*CTNs and *h*CTNs/PANI electrode is ~100% and ~75%, respectively (Fig. 5f). The lower capacitance retention of *h*CTNs/PANI electrode can be attributed to relatively poor stability and partial degradation of PANI.

## 4. Conclusion

In summary, a highly stretchable supercapacitor electrode has been successfully designed and constructed through employing *h*CTNs/PANI composites as electrode material and stainless steel spring as substrate. The resultant helical electrodes not only possess considerable stretchability and mechanical flexibility, but also exhibit excellent linear capacitance of 402.8 mF cm$^{-1}$ and good cyclic stability (75% capacitance retention over 3000 charge-discharge cycles). These encouraging results presented here may pave a way for the fabrication of novel stretchable energy storage devices.

## Acknowledgements

We are thankful to Shengnian Luo and Analytical and Testing Center of Southwest Jiaotong University for supporting the SEM measurements and TEM characterization. This work is supported by the National Natural Science Foundation of China (No. 51602265), the Scientific and Technological Projects for Distinguished Young Scholars of Sichuan Province (No. 2015JQ0013), China Postdoctoral Science Foundation (2016M592692), and the Fundamental Research Funds for the Central Universities of China (A0920502051619-72) and the Independent Research Project of State Key Laboratory of Traction Power (Nos. 2017TPL_Z04, 2016TPL_Z03).

## Appendix A. Supplementary data

Supplementary data associated with this article can be found, in the online version, at http://dx.doi.org/10.1016/j.cej.2018.05.090.

## References

[1] Y. Wang, Y. Song, Y. Xia, Electrochemical capacitors: mechanism, materials, systems, characterization and applications, Chem. Soc. Rev. 45 (2016) 5925–5950.
[2] X. Lu, M. Yu, G. Wang, Y. Tong, Y. Li, Flexible solid-state supercapacitors: design, fabrication and applications, Energy Environ. Sci. 7 (2014) 2160.
[3] P. Simon, Y. Gogotsi, Materials for electrochemical capacitors, Nat. Mater. 7 (2008) 845–854.
[4] H.P. Cong, X.C. Ren, P. Wang, S.H. Yu, Flexible graphene–polyaniline composite paper for high-performance supercapacitor, Energy Environ. Sci. 6 (2013) 1185.
[5] K. Wang, P. Zhao, X. Zhou, H. Wu, Z. Wei, Flexible supercapacitors based on cloth-supported electrodes of conducting polymer nanowire array/SWCNT composites, J. Mater. Chem. 21 (2011) 16373.
[6] D. Son, J. Lee, S. Qiao, R. Ghaffari, J. Kim, J.E. Lee, C. Song, S.J. Kim, D.J. Lee, S.W. Jun, S. Yang, M. Park, J. Shin, K. Do, M. Lee, K. Kang, C.S. Hwang, N.S. Lu, T. Hyeon, D.H. Kim, Multifunctional wearable devices for diagnosis and therapy of movement disorders, Nat. Nanotechnol. 9 (2014) 397–404.
[7] L. Jin, W. Deng, Y. Su, Z. Xu, H. Meng, B. Wang, H. Zhang, B. Zhang, L. Zhang, X. Xiao, M. Zhu, W. Yang, Self-powered wireless smart sensor based on maglev porous nanogenerator for train monitoring system, Nano Energy 38 (2017) 185–192.
[8] L. Jin, J. Chen, B.B. Zhang, W.L. Deng, L. Zhang, H.T. Zhang, X. Huang, M.H. Zhu, W.Q. Yang, Z.L. Wang, Self-powered safety helmet based on hybridized nanogenerator for emergency, ACS Nano 10 (2016) 7874–7881.
[9] K. Wang, W. Zou, B. Quan, A. Yu, H. Wu, P. Jiang, Z. Wei, An all-solid-state flexible micro-supercapacitor on a chip, Adv. Energy Mater. 1 (2011) 1068–1072.
[10] W. Xu, Z. Jiang, Q. Yang, W. Huo, M.S. Javed, Y. Li, L. Huang, X. Gu, C. Hu, Approaching the lithium-manganese oxides' energy storage limit with Li2MnO3 nanorods for high-performance supercapacitor, Nano Energy 43 (2018) 168–176.
[11] S. Dai, W. Xu, Y. Xi, M. Wang, X. Gu, D. Guo, C. Hu, Charge storage in KCu7S4 as redox active material for a flexible all-solid-state supercapacitor, Nano Energy 19 (2016) 363–372.
[12] Y.X. Xu, Z.Y. Lin, X.Q. Huang, Y. Liu, Y. Huang, X.F. Duan, Flexible solid-state supercapacitors based on three-dimensional graphene hydrogel films, ACS Nano 7 (2013) 4042–4049.
[13] A. Lamberti, F. Clerici, M. Fontana, L. Scaltrito, A highly stretchable supercapacitor using laser-induced graphene electrodes onto elastomeric substrate, Adv. Energy Mater. 6 (2016) 1600050.
[14] Z. Yang, J. Deng, X. Chen, J. Ren, H. Peng, A highly stretchable, fiber-shaped supercapacitor, Angew. Chem. Int. Edit. 52 (2013) 13453–13457.
[15] Z. Zhang, L. Wang, Y. Li, Y. Wang, J. Zhang, G. Guan, Z. Pan, G. Zheng, H. Peng, Nitrogen-doped core-sheath carbon nanotube array for highly stretchable supercapacitor, Adv. Energy Mater. 7 (2017) 1601814.
[16] S.E. Moosavifard, J. Shamsi, M.K. Altafi, Z.S. Moosavifard, All-solid state, flexible, high-energy integrated hybrid micro-supercapacitors based on 3D LSG/CoNi2S4 nanosheets, Chem. Commun. 52 (2016) 13140–13143.
[17] X. Dong, Z. Guo, Y. Song, M. Hou, J. Wang, Y. Wang, Y. Xia, Flexible and wire-shaped micro-supercapacitor based on Ni(OH)2-nanowire and ordered mesoporous carbon electrodes, Adv. Funct. Mater. 24 (2014) 3405–3412.
[18] Y. Xie, Y. Liu, Y. Zhao, Y.H. Tsang, S.P. Lau, H. Huang, Y. Chai, Stretchable all-solid-state supercapacitor with wavy shaped polyaniline/graphene electrode, J. Mater. Chem. A 2 (2014) 9142–9149.
[19] B. Yue, C. Wang, X. Ding, G.G. Wallace, Polypyrrole coated nylon lycra fabric as stretchable electrode for supercapacitor applications, Electrochim. Acta 68 (2012) 18–24.
[20] Y. Huang, H. Hu, Y. Huang, M.S. Zhu, W.J. Meng, C. Liu, Z.X. Pei, C.L. Hao, Z.K. Wang, C.Y. Zhi, From industrially weavable and knittable highly conductive yarns to large wearable energy storage textiles, ACS Nano 9 (2015) 4766–4775.
[21] K. Krishnamoorthy, P. Pazhamalai, G.K. Veerasubramani, S.J. Kim, Mechanically delaminated few layered MoS2 nanosheets based high performance wire type solid-state symmetric supercapacitors, J. Power Sources 321 (2016) 112–119.
[22] P. Sun, R. Lin, Z. Wang, M. Qiu, Z. Chai, B. Zhang, H. Meng, S. Tan, C. Zhao, W. Mai, Rational design of carbon shell endows TiN@C nanotube based fiber supercapacitors with significantly enhanced mechanical stability and electrochemical performance, Nano Energy 31 (2017) 432–440.
[23] M. Hu, Y. Liu, M. Zhang, H. Wei, Y. Gao, Wire-type MnO2/multilayer graphene/Ni electrode for high-performance supercapacitors, J. Power Sources 335 (2016) 113–120.
[24] H. Zhang, H. Su, L. Zhang, B. Zhang, F. Chun, X. Chu, W. He, W. Yang, Flexible supercapacitors with high areal capacitance based on hierarchical carbon tubular nanostructures, J. Power Sources 331 (2016) 332–339.
[25] H. Zhang, X. Zhang, X. Sun, Y. Ma, Shape-controlled synthesis of nanocarbons through direct conversion of carbon dioxide, Sci. Rep. 3 (2013) 3534.
[26] X. Chen, F. Meng, Z. Zhou, X. Tian, L. Shan, S. Zhu, X. Xu, M. Jiang, L. Wang, D. Hui, Y. Wang, J. Lu, J. Gou, One-step synthesis of graphene/polyaniline hybrids by in situ intercalation polymerization and their electromagnetic properties, Nanoscale 6 (2014) 8140–8148.
[27] H. Fan, H. Wang, N. Zhao, X. Zhang, J. Xu, Hierarchical nanocomposite of polyanilinenanorods grown on the surface of carbon nanotubes for high-performance supercapacitor electrode, J. Mater. Chem. 22 (2012) 2774–2780.
[28] G.M. Zhou, D.W. Wang, F. Li, L.L. Zhang, Z. Weng, H.M. Cheng, The effect of carbon particle morphology on the electrochemical properties of nanocarbon/polyaniline composites in supercapacitors, New Carbon Mater. 26 (2011) 180–186.
[29] H. Zhang, X. Zhang, Y. Ma, Enhanced capacitance supercapacitor electrodes from porous carbons with high mesoporous volume, Electrochim. Acta 184 (2015) 347–355.
[30] H. Su, H. Zhang, F. Liu, F. Chun, B. Zhang, X. Chu, H. Huang, W. Deng, B. Gu, H. Zhang, X. Zheng, M. Zhu, W. Yang, High power supercapacitors based on hierarchically porous sheet-like nanocarbons with ionic liquid electrolytes, Chem. Eng. J. 322 (2017) 73–81.
[31] H. Zhang, X. Zhang, X. Sun, D. Zhang, H. Lin, C. Wang, H. Wang, Y. Ma, Large-scale production of nanographene sheets with a controlled mesoporous architecture as high-performance electrochemical electrode materials, ChemSusChem 6 (2013) 1084–1090.
[32] H. Zhang, K. Wang, X. Zhang, H. Lin, X. Sun, C. Li, Y. Ma, Self-generating graphene and porous nanocarbon composites for capacitive energy storage, J. Mater. Chem. A 3 (2015) 11277–11286.
[33] K. Wang, X. Zhang, C. Li, X. Sun, Q. Meng, Y. Ma, Z. Wei, Chemically crosslinked hydrogel film leads to integrated flexible supercapacitors with superior performance, Adv. Mater. 27 (2015) 7451–7457.
[34] Y. Shi, L. Pan, B. Liu, Y. Wang, Y. Cui, Z. Bao, G. Yu, Nanostructured conductive polypyrrole hydrogels as high-performance, flexible supercapacitor electrodes, J. Mater. Chem. A 2 (2014) 6086.
[35] V.T. Le, H. Kim, A. Ghosh, J. Kim, J. Chang, Q.A. Vu, D.T. Pham, J.H. Lee, S.W. Kim, Y.H. Lee, Coaxial fiber supercapacitor using all-carbon material electrodes, ACS Nano 7 (2013) 5940–5947.